Polaronic interactions between oxygen vacancies in rutile TiO_2

Liang Zhao, Blanka Magyari-Köpe, and Yoshio Nishi
Department of Electrical Engineering, Stanford University, Stanford, California 94305, USA
(Received 5 October 2013; revised manuscript received 18 August 2016; published 6 February 2017)

Oxygen vacancy-vacancy interactions in rutile TiO_2 are studied in conjunction with polaron formation trends using density functional theory calculations. It is found that polarons strongly enhance the formation of oxygen vacancies in this material and also mediate the interactions between existing vacancies. At distances below 1 nm, two isolated and charge-neutral vacancies exhibit attractive interactions with an equilibrium distance of about 4 Å. The attractive forces between vacancies partly arise from the polaronic transfer of excess electrons to reduce the potential energy. These discoveries provide microscopic explanations to the vacancy clustering phenomena, as well as a practical approach to stabilize the polarons at arbitrary Ti atoms in TiO_2.

DOI: 10.1103/PhysRevB.95.054104

I. INTRODUCTION

Recently, titanium oxide nanomaterials have been widely investigated for a range of applications including photocatalysis [1–5], solar energy conversion [6,7], and nanoelectronic devices such as high-k gate dielectrics [8] and resistive random-access memories (RRAM) [9–12]. The conductivity of titanium oxide varies significantly in these applications, which is affected by factors such as nonstoichiometry, crystallinity, and surface morphology. Especially, an increased level of bulk n-type conductivity is often observed without the intentional introduction of dopants during the fabrication process [13–15]. Therefore, the n-type semiconducting behaviors have traditionally been attributed to the presence of oxygen vacancies (V_O), which contribute excess electrons to the lattice [13–17]. However, the nature of these excess electrons still remains a matter of active debate due to the widely observed electron self-trapping phenomena, i.e., the polaronic effects in titanium oxide. In pristine TiO_2, the small-polaron model has been proposed to describe the excess electrons localized around Ti atoms [18], supported by recent electron spin resonance (ESR) measurements [19]. Nevertheless, in the presence of oxygen vacancies (V_O), the picture becomes more complex, and recent studies suggest the coexistence of both small polarons and delocalized electrons [17].

As the oxygen-vacancy concentration increases, titanium oxide eventually becomes metallic due to the clustering of these point defects. Long-range order of vacancies leads to crystallographic shear and transformation into the Magnéli phases (Ti_nO_{2n-1}, $n > 3$ [20]). These substoichiometric phases have been widely observed in TiO_2 thin films [11], nanoparticles [21], and nanowires [22]. Due to the metallic conductivity, they have been widely considered as possible electrode materials in batteries and fuel cells [23–25]. The desirable chemical stability and abundant low-temperature behaviors of Magnéli phases also generated substantial research interests lately [26–30]. For example, various bipolaron models have been proposed to explain the two-step metal-insulator transitions of Ti_4O_7 between 125 and 150 K [28–30].

In previous studies, the isolated and clustered oxygen vacancies in titanium oxide have been investigated separately and it is still unclear how a pair of oxygen vacancies will interact when they come close to each other. Although it has been suggested that clustered vacancies have lower energies compared to isolated vacancies in the neutral charge state [31,32], the effects of multiple polaronic states were not thoroughly considered. Moreover, during the approaching of two oxygen vacancies, the redistribution of charges coupled with the structural change has never been fully investigated. In this work, we report an in-depth study of the vacancy-vacancy interactions in rutile TiO_2 based on density functional theory (DFT) and an extensive search of potential polaronic states. The total energy of the system in each polaronic state has been calculated to identify the ground state at various vacancy-vacancy distances and to characterize the potential energy surface. Our results suggest that two isolated V_O in rutile TiO_2 exhibit attractive interactions with an equilibrium distance of about 4 Å. The attractive forces between vacancies arise from the polaronic effects which redistribute the excess electrons to minimize their Coulomb repulsion. These insights provide an in-depth understanding of the vacancy clustering process from a microscopic point of view.

II. METHODS

Theoretical studies of defect states with DFT are challenging since the standard local/semilocal approximations such as local density approximation (LDA) and generalized gradient approximation (GGA) severely underestimate the bandgap of TiO_2 and suppress the polaron formation [31]. In order to reproduce the correct polaronic behaviors, the self-interaction of electrons must be treated properly to balance the tendency of localization versus delocalization [33–44]. Hybrid functionals [33–40] and on-site Coulomb corrections [31,32,41–44] are two potential treatments. Using hybrid functionals, several groups of researchers have reported the coexistence of two distinct polaronic states [17,35–38]. The first state is the widely observed closed-shell solution, which has two electrons distributed in between three Ti neighbors [35–37]. The Kohn-Sham (KS) energy level of this defect state is relatively deep (0.4–1.0 eV below the conduction band minimum [17,33,36,40–45]), in contrast to the experimentally observed shallow donor states [46–49]. Thus, they are unlikely to be the major contributor of n-type conductivity in rutile TiO_2. On the other hand, the second state reported has two excess electrons localized at two neighboring Ti sites in the form of electron polarons [17,36,39]. This state, only

discovered recently by hybrid-functional calculations, was predicted to be more stable over the first one [17,36].

Hybrid-functional calculations usually require one order of magnitude more computational resources than standard DFT [50], limiting their application to systems with no more than a few hundred atoms. In this work, an alternative approach has been adopted to study the polaronic states in rutile TiO_2, which is DFT with on-site Coulomb corrections (DFT + U). Our previous calculations confirmed its capability to reproduce the correct band gap and lattice constants of TiO_2 [31]. Here the exact cancellation of self-interaction errors is further verified by checking the "generalized Koopmans' condition" [33–36]. The finely tuned corrections were then applied to calculate the polaronic states in pristine and oxygen-deficient TiO_2. Qualitative agreements were observed with the previously reported hybrid-functional calculations but were obtained at a much-reduced computational cost.

The predicted ground states of an isolated V_O are found to be consistent with the recently reported experimental results by electron spin resonance [46–48]. By considering the polaronic effects, the defect levels of an isolated vacancy become significantly shallower ($\Leftarrow$ 0.1 eV), which provides a more consistent explanation for the n-type conductivity in TiO_2. With a consistent description of an isolated V_O, the methodology was then applied to study the vacancy-vacancy interactions. By varying the distance between a pair of V_O, the changes of thermodynamic stability and electronic structures in various polaronic states are thoroughly discussed.

The DFT calculations were carried out using density functional theory as implemented in the Vienna *ab initio* simulation package (VASP [51]), in which the projector-augmented-wave pseudopotentials were employed [52]. For K-point sampling, a $2 \times 2 \times 2$ Monkhorst-Pack grid in the first Brillouin zone was applied. All calculations were based on a $3 \times 3 \times 4$ supercell of rutile TiO_2 with a total of 216 atoms. The atomic relaxations were performed until the force on each atom was reduced to $<$0.005 eV/Å with a plane-wave cut-off energy of 353 eV. The exchange and correlation energy of electrons is described with LDA + U [53]. In order to overcome the underestimation of bandgap by LDA, on-site Coulomb corrections to both O 2p orbitals and Ti 3d orbitals were applied (LDA + U^d + U^p). Here we use 8 eV for U^d, 6 eV for U^p, and 0.6 eV for the exchange parameter J, which adequately reproduced the electronic structures and lattice constants of rutile TiO_2 [31]. These parameters are consistent with the values obtained by proper rescaling of U values of single ions (calculated by DFT) to fit the electronic bandgap of TiO_2 [43]. The importance of applying U to O-2p in addition to Ti-3d states was discussed elsewhere [31,43,54].

Compared to the widely studied hybrid-functional method [17,35–38], DFT + U has significantly better computational efficiency, making it favorable for the studies of large systems and multiple polaronic states. On the other hand, DFT + U may be less accurate for the treatment of electron-electron correlation effects, and the choice of U values requires extra caution. In this work, the choice of U values followed our previous work, which examined various U^d-U^p combinations and their effects on the geometry and band structures of rutile TiO_2 [31]. Here we further verify the capability of our model to properly describe the electron self-interaction by checking

TABLE I. Fulfillment of the generalized Koopmans' condition by LDA + U^d + U^p approach. (Energies refer to the valence band maximum.)

Defect type	$e_i(N)$ (eV)	$E(N)$-$E(N\text{-}1)$ (eV)
Rutile V_O	2.097	2.193
Rutile Al_{Ti}	0.036	0.022

the "generalized Koopmans' condition" (gKC) [33–36]. The gKC states that, in order to fully eliminate the self-interaction errors associated with the exchange-correlation functional, the K-S level of the defect state should be equal to the electron addition/removal energy of the system. When the gKC is satisfied, the linear behavior of total energy as a function of fractional occupation number is retained. In this work, we follow the procedure described by Deak *et al.* [35] to verify gKC. As shown in Table I, the fulfillment of gKC is confirmed to be within 0.1 eV for both oxygen vacancy and Al dopant [55].

In contrast to the empirical determination of U, there are more rigorous ways to compute U fully *ab initio*, such as the constrained random phase approximation (cRPA) [56] or the linear response approach by Cococcioni and Gironcoli [57]. However, these methods often lead to lower U^d values and an underestimated band gap. In order to achieve the correct band gap for TiO_2, a relatively high U^d value for Ti is needed, which enhances the tendency of electron localization and polaron formation at Ti sites. In general, it would be interesting to

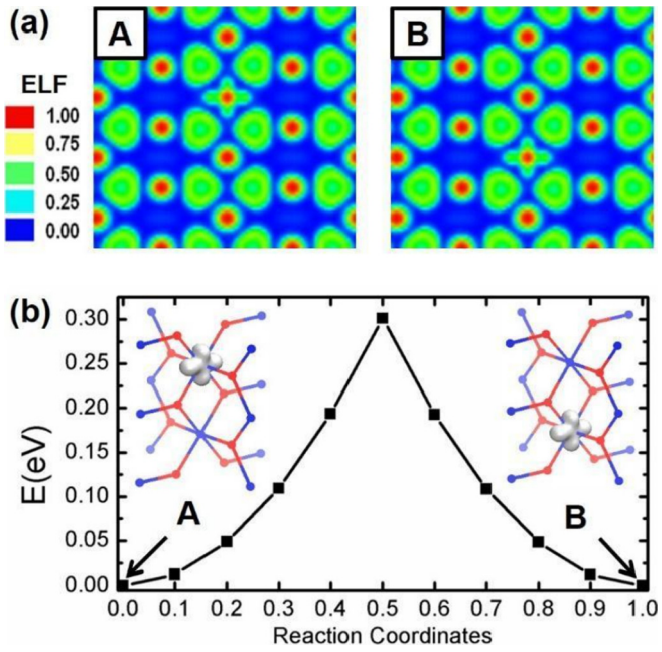

FIG. 1. (a) Electron localization functions (ELFs) which demonstrate small polarons formed at two different Ti atomic sites. (b) Energies of the polaron migration pathway between A and B, calculated by linear interpolation of atomic positions. Insets: the isosurface plot of partial charge densities (isosurface density is 0.1 electrons/Å^3), representing the small-polaron localization at different Ti sites.

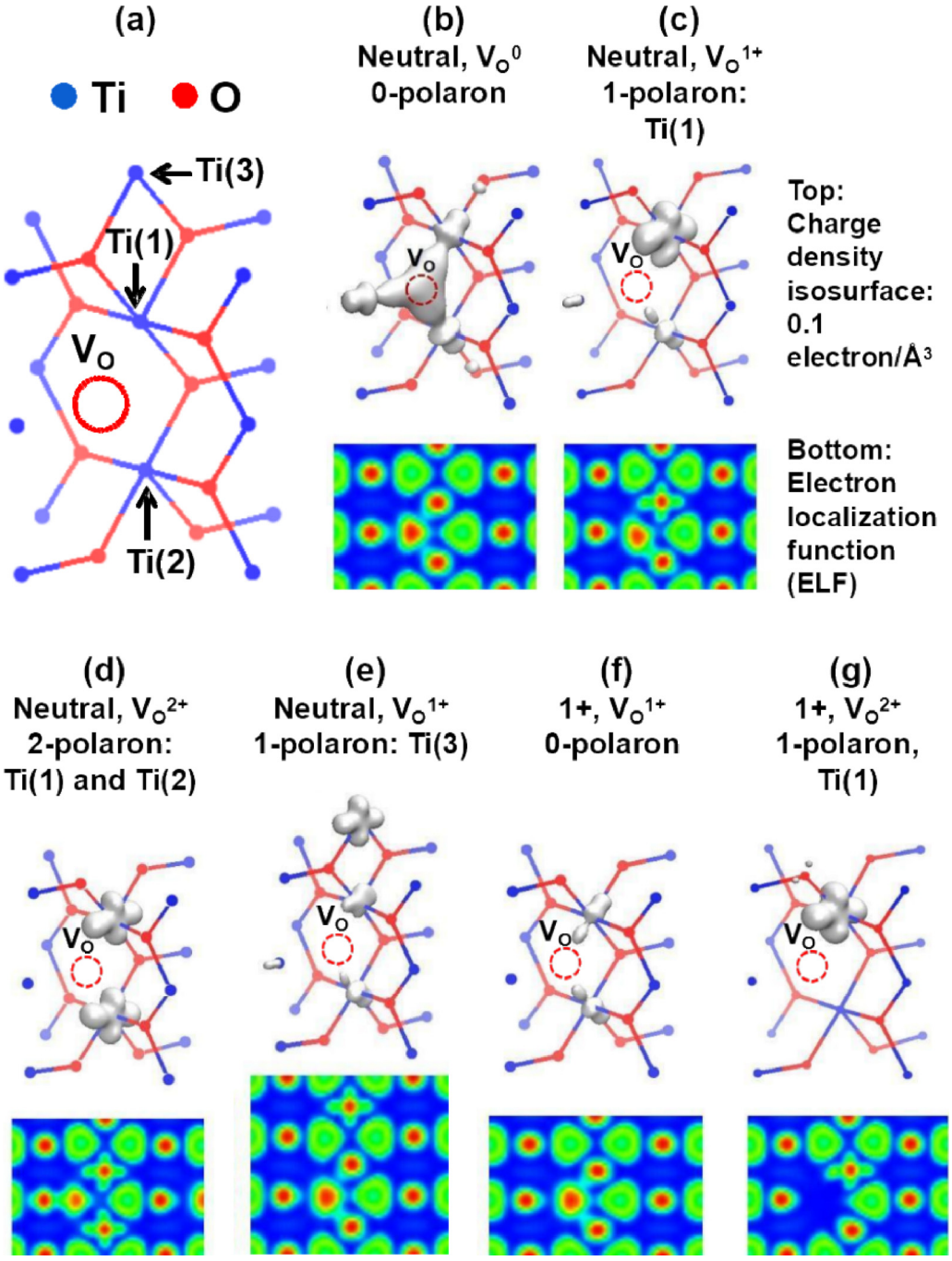

FIG. 2. (a) The atomic configuration of a single V_O in rutile TiO_2. (b–g) The isosurface plots of partial charge densities (top row) and the electron localization functions of the spin-up states (bottom row) of various configurations: (b) neutral, V_O^0, 0-polaron; (c) neutral, V_O^{1+}, 1-polaron, Ti(1); (d) neutral, V_O^{2+}, 2-polaron, Ti(1) and Ti(2); (e) neutral, V_O^{1+}, 1-polaron, Ti(3); (f) 1+, V_O^{1+}, 0-polaron; (g) 1+, V_O^{2+}, 1-polaron, Ti(1).

examine the polaronic behaviors of TiO_2 at various U values, which is beyond the scope of this study.

III. POLARONIC STATES OF AN ISOLATED OXYGEN VACANCY

Figure 1(a) demonstrates the electron localization functions (ELFs) indicating a small polaron localized at two different Ti sites in rutile TiO_2. The ELF is a powerful tool to identify polaron formation, which has a value between 0 and 1 that characterizes the type of chemical bonding in the space [58]. The cross-shaped charge localization is a signature of the electron polaron at the Ti atomic sites. As a benchmark, we further simulated the migration of a small polaron by linear interpolation of the atomic positions [17,59–61]. The nonadiabatic polaron transfer energy in rutile [001] direction is calculated to be around 0.30 eV [Fig. 1(b)], consistent with previous GGA + U calculation [59].

TABLE II. Formation energies of the isolated V_O in various polaronic states

Charge state	Polaronic state	Formation energy (eV)
Neutral	V_O^0, 0-polaron	3.203
	V_O^{1+}, 1-polaron, Ti(1)	2.768
	V_O^{2+}, 2-polaron, Ti(1) and Ti(2)	2.490
	V_O^{1+}, 1-polaron, Ti(3)	2.978
1+	V_O^{1+}, 0-polaron	3.542
	V_O^{2+}, 1-polaron, Ti(1)	3.177

With consistent results on a small polaron, we moved on to study the polaronic states of a single V_O. With the creation of one V_O, two excess electrons are contributed to the system. Figure 2(a) depicts the atomic configuration of the single V_O. Here we define the two nearest-neighboring Ti atoms in the diagonal direction as Ti(1) and Ti(2), and a non-neighboring Ti atom as Ti(3). We adopt the following criteria to distinguish the polaronic states:

(i) The charge state of the whole system: neutral, 1+, 2+;

(ii) The charge state of the V_O [17], considering the number of electrons that occupy a defect state whose density is centered on the V_O: V_O^0, V_O^{1+}, V_O^{2+};

(iii) The number of polarons localized on Ti atoms: 0 polaron, 1 polaron, or 2 polaron; and

(iv) The location of Ti sites at which each polaron is localized: Ti(1), Ti(2), or Ti(3).

In a previous study, we reported one defect state with both electrons localized in the vacancy without the formation of small polarons [31]. As shown in Fig. 2(b), this case is denoted as the "neutral, V_O^0, 0-polaron" state. In addition, we discovered that two other polaronic states can be stabilized after relaxation by manually changing the initial atomic positions. As shown in Figs. 2(c) and 2(d), these two configurations correspond to the formation of one and two polarons, respectively. The calculated formation energies of V_O (Table II) indicate that the "neutral, V_O^{2+}, 2-polaron, Ti(1) and Ti(2)" state is the most stable one, while the "neutral, V_O^0, 0-polaron" and "neutral, V_O^{1+}, 1-polaron, Ti(1)" states are metastable. Recently, ESR studies on the triplet ground state of neutral V_O in rutile TiO_2 confirmed that the two electrons trapped by V_O are localized on two separate Ti neighbors, forming a pair of exchange-coupled Ti^{3+} ions aligned along the [001] direction [46]. Thus, the simulations indicated the correct polaronic ground state of neutral V_O among the three possible solutions, in perfect agreement with experimental results. Figure 2(e) shows the metastable configuration with one polaron formed and migrated to a non-neighboring Ti atom, Ti(3). Compared to Fig. 2(c), the formation energy of the migrated-polaron configuration is higher, which can be attributed to the attractive Coulomb interactions between the electron polaron and the positively charged (1+) V_O. These observations suggest that an isolated oxygen vacancy tends to form bound polarons in a neutral charge state [46].

In the 1+ charge state, on the other hand, two possible polaronic states were found after atomic relaxations, as shown in Figs. 2(f) and 2(g). Following similar notations they are denoted as "1+, V_O^{1+}, 0-polaron" and "1+, V_O^{2+}, 1-polaron, Ti(1)," respectively. The "1+, V_O^{2+}, 1-polaron, Ti(1)" state has a lower formation energy, which is consistent with the ESR results of the singlet ground state of a positively charged oxygen vacancy [49]. Furthermore, the electron densities of this singlet state is roughly half of the electron densities of the triplet ground state in the neutral charge state, which explains why the hyperfine matrix **A** of the triplet state is approximately twice that of the singlet state, as found by ESR [46,49].

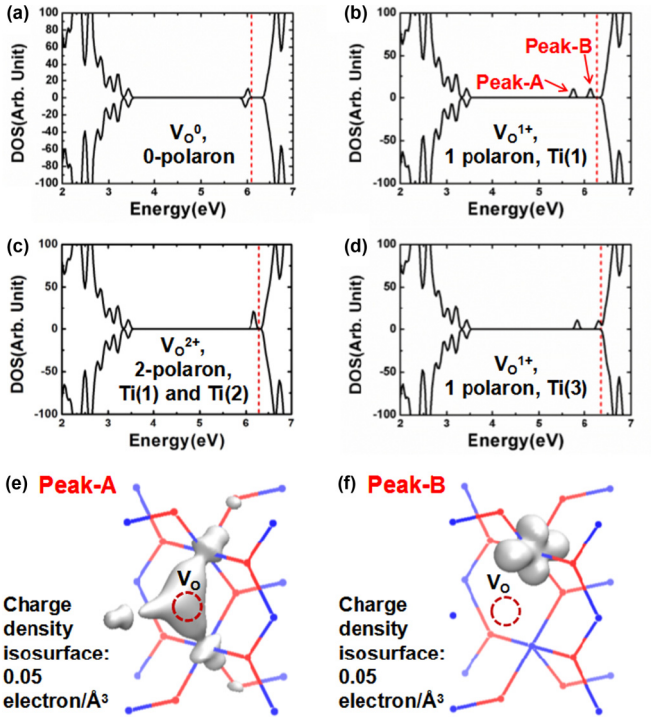

FIG. 3. (a–d) Electron spin density of states (DOS) of the following configurations: (a) neutral, V_O^0, 0-polaron; (b) neutral, V_O^{1+}, 1-polaron, Ti(1); (c) neutral, V_O^{2+}, 2-polaron, Ti(1) and Ti(2); (d) neutral, V_O^{1+}, 1-polaron, Ti(3). The Fermi level is represented by red dashed lines. (e–f) Charge-density isosurface plots of (e) peak A and (f) peak B of the "neutral, V_O^{1+}, 1-polaron, Ti(1)" state.

Figures 3(a)–3(d) show the electron density of states (DOS) for the configurations in Figs. 2(b)–2(e). The "neutral, V_O^0, 0-polaron" configuration has a defect state at 0.4 eV below the bandgap, consistent with Ref. [31]. The "neutral, V_O^{1+}, 1-polaron, Ti(1)" configuration has the defect state split into two levels that are 0.36 eV apart, with the upper level at 0.21 eV below the conduction band minimum (CBM). The "neutral, V_O^{2+}, 2-polaron, Ti(1) and Ti(2)" configuration restores the single defect level again, which is now only 0.1 eV below CBM. When one polaron is formed and migrated away from the vacancy as shown in Fig. 3(d), the defect state is split further by 0.48 eV, while the upper level begins to merge with CBM. To further demonstrate the nature of the two defect levels in Figs. 3(b) and 3(d), the peak-resolved charge isosurfaces are plotted in Figs. 3(e) and 3(f) for "neutral, V_O^{1+}, 1-polaron, Ti(1)." It is verified that the deeper defect level (peak A) corresponds to charge densities centered on V_O, while the shallower defect level (peak B) corresponds to the polaron localized on Ti(1). It is worth noting that the defect level of the small polaron is much shallower

TABLE III. The atomic distances around one single oxygen vacancy in rutile TiO_2 with various polaronic states.[a]

Charge state	Polaronic state	Atomic pair no.	Ti-Ti distances around V_O (Å) 1	2	3	Ti-O distances around Ti(1) (Å) 4	5	6	7	8	Ti-O distances around Ti(2) (Å) 9	10	11	12	13
Neutral	Pristine TiO_2		3.54	3.54	2.99	1.95	1.95	1.95	1.95	1.95	1.95	1.95	1.95	1.95	1.95
	V_O^0, 0-polaron		3.64	3.64	3.01	1.99	1.96	1.96	1.95	1.95	1.99	1.96	1.96	1.95	1.95
	V_O^{1+}, 1-polaron, Ti(1)		3.73	3.78	3.11	2.03	1.98	2.01	1.98	1.98	1.97	1.93	1.89	1.95	1.95
	V_O^{2+}, 2-polaron, Ti(1) and Ti(2)		3.94	3.94	3.23	2.03	1.95	1.96	1.98	1.98	2.03	1.95	1.96	1.98	1.98
	V_O^{1+}, Ti(3)		3.78	3.81	3.15	1.94	1.9	1.92	1.94	1.94	1.9	1.84	1.94	1.95	1.95
1+	V_O^{1+}, 0-polaron		3.79	3.79	3.15	1.94	1.89	1.92	1.94	1.94	1.94	1.89	1.92	1.94	1.94
	V_O^{2+}, 1-polaron, Ti(3)		3.92	4.02	3.27	2.03	1.95	2.00	1.97	1.97	1.93	1.81	1.88	1.93	1.93

[a]The number of atomic pairs is labeled in Fig. 4.

compared to that calculated by the hybrid functional [17]. This discrepancy could potentially be attributed to the local nature of U. It is also worth mentioning that the Fermi levels of these systems are elevated compared to pristine TiO_2, generating larger electron concentration near CBM. These results further support the bound-polaron picture of the shallow donor states induced by oxygen vacancies, and also explains the significant enhancement of UV absorption by reduced TiO_2 in photocatalysis [62,63].

Since a polaron is essentially a localized electronic state bound by the electron-phonon interactions, it is expected that multiple metastable states exist, especially in the presence of oxygen vacancies which disrupt the local symmetry. In this study, the atomic coordinates in all polaronic states of one oxygen vacancy are summarized in Table III. When no polaron is formed, the surrounding Ti-Ti distances are slightly larger compared to pristine TiO_2. When one electron polaron is formed at Ti(1), the Ti-O distances around this Ti atom are stretched due to enhanced Coulomb repulsion, breaking also the symmetry between Ti(1) and Ti(2) and causing the split of DOS in Fig. 3(b). At the same time, the Ti-Ti distances around the V_O become larger due to the decrease of negative charges at the vacancy site, which mitigates the Coulomb repulsion among Ti cations. Similarly, when a second polaron is formed, the Ti-Ti distances around the V_O are further stretched. The energy required to achieve these lattice distortions is compensated by the reduced Coulomb energy through the spatial and orbital redistributions (e_g to t_{2g}) of electrons.

In *ab initio* studies of polaronic states, different strategies can be adopted to trap the polarons at specific sites, such as manual structural modifications [64,65], using vacancy substitutions [66], or setting different values for the on-site U [67]. The information from Table III can act as a guideline for manual structural modification to stabilize arbitrary polaron states. A similar but less systematic approach has been explored recently to stabilize a bipolaron state on the surface of rutile TiO_2 [65].

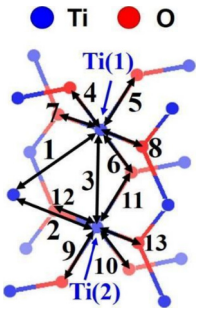

FIG. 4. Numbered atomic pairs around the single V_O. The corresponding atomic distances are summarized in Table III.

IV. VACANCY-VACANCY INTERACTIONS

As two V_O's approach each other, the excess electrons and corresponding lattice distortions will start to interact. An extreme case is when the two V_O migrate into the same TiO_6 octahedron and share one Ti atom as their nearest neighbor. In this work, we studied all five nonequivalent configurations that belong to this category [labeled C1–C5, as shown in Fig. 5(a)]. The TiO_6 octahedron is the basic building block of

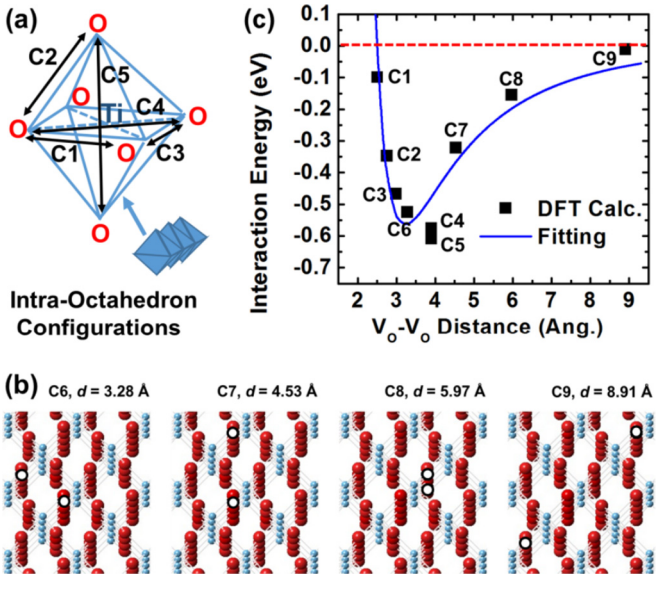

FIG. 5. (a) Schematics of the five configurations of which the two V_O are located in the same TiO_6 octahedron (C1–C5). (b) Schematics of the four configurations of which the two V_O are located in different TiO_6 octahedra (C6–C9). The oxygen vacancies are represented by black circles. (c) The interaction energies between two oxygen vacancies in each of these configurations with respect to the noninteractive case.

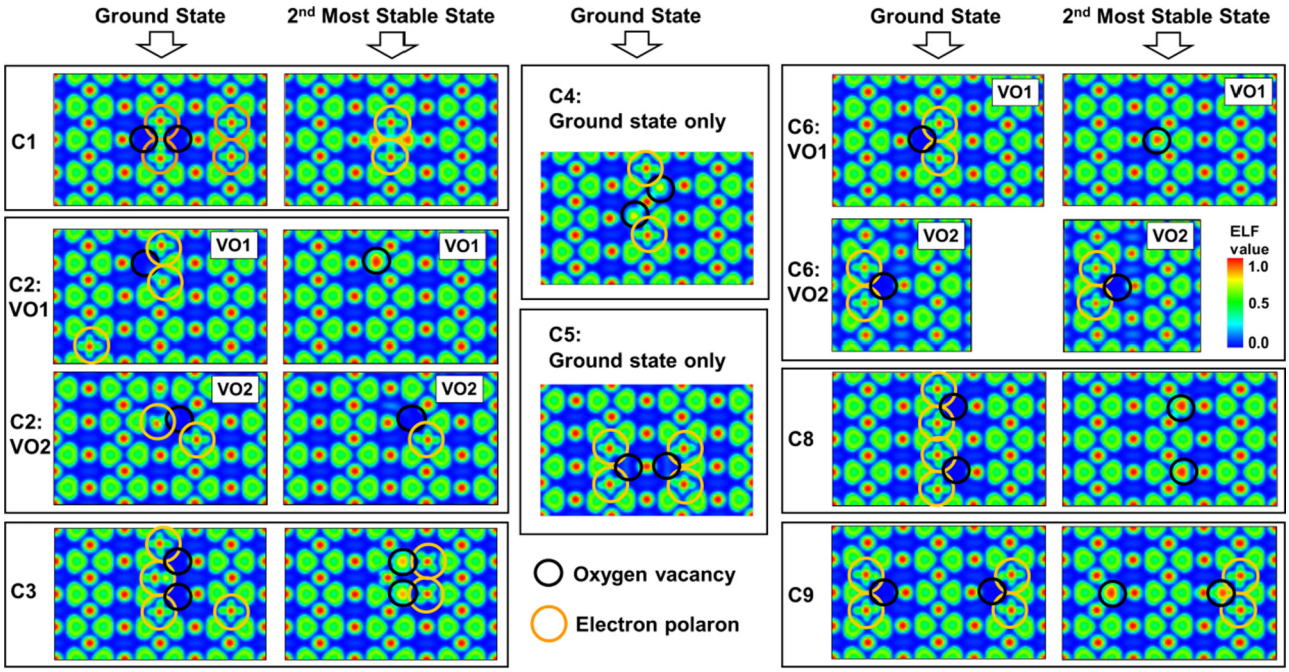

FIG. 6. The ELFs of the ground states of C1–C9 and the second-most-stable polaronic states of C1–C3 and C6–C9 (excluding C7). The results for C7 are not included because they looked almost exactly the same as C6. The black circles represent the locations of oxygen vacancies, and the golden circles represent small polarons localized at Ti atoms.

various crystal structures of TiO_2, including rutile, anatase, and brookite. In addition, four other double-vacancy configurations with the two V_O located in separate TiO_6 octahedra were studied [labeled C6–C9, see Fig. 5(b)]. The supercell with only one V_O is referred to as the noninteractive case, i.e., when the V_O-V_O distance is very large.

Based on the atomic relaxation data from Table III, all the double-vacancy configurations were positioned into nine different polaronic states (three polaronic states for each V_O). These initial configurations were then fully relaxed to search for the ground states. To determine the most stable configurations, the interaction energy (E_{int}) is calculated with respect to the noninteractive reference using the following formula:

$$E_{int} = E_{2V_O} + E_{TiO_2} - 2E_{1V_O}, \quad (1)$$

where E_{TiO_2} is the total energy of the pristine supercell and E_{1V_O}, E_{2V_O} are the total energies of the supercell, including one or two vacancies, respectively. The polaronic states with the lowest interaction energies are identified as the ground state of each configuration, and Fig. 5(c) shows the calculated E_{int} of each configuration's ground state, plotted as a function of the V_O-V_O distances.

According to Fig. 5(c), the interaction energies of all configurations are calculated to be negative. This suggests that two isolated V_O exhibit attractive interaction when they approach each other. A simplified way to understand this attractive interaction is to view the oxygen vacancy and its excess electrons as a dipole. When this dipole approaches an ion or another dipole, its direction and amplitude can be adjusted through the redistribution of excess electrons. The distance dependence of such charge-dipole and dipole-dipole interactions can be estimated as $\sim 1/r^2$ and $\sim 1/r^6$, respectively [68].

When the distance between two V_O becomes very small, they can no longer be treated as two free-rotating dipoles. Instead, the space between them is too small for all the excess electrons to freely redistribute, as in the case of C1–C5. Thus, the Coulomb repulsion between two positively charged vacancies should become stronger, as they cannot be fully mediated by excess electrons. This argument is confirmed by the calculation results of C1–C5, as E_{int} increases with decreasing V_O-V_O distance. Among them, the most stable configurations are C4 and C5. The two V_O in these cases are located in the opposite directions of the Ti atom, with V_O-Ti-V_O angles of 180 deg. On the other hand, C1–C3 have V_O-Ti-V_O angles of approximately 90 deg. Among them, C3 has the largest V_O-V_O distance and also the lowest interaction energy. The distance dependence of unscreened Coulomb repulsion is $\sim 1/r$. Thus, the interaction energies are fitted with the following equation to verify the proposed physical mechanisms:

$$E_{int}(r) = A/r - B/r^2 - C/r^6. \quad (2)$$

As shown in Fig. 5(c), a satisfactory fitting result is obtained, with $A = 0.753\,\text{eV/Å}$, $B = 11.83\,\text{eV/Å}^2$, and $C = -383.45\,\text{eV/Å}^6$. Now, this set of parameters can be applied to evaluate V_O-V_O interactions in TiO_2 beyond *ab initio* calculations.

In order to reveal the microscopic origin of the interactions between vacancies, we further analyzed the electronic wave functions by plotting the ELF. Figure 6 compares the ELF of the ground states and the second-most-stable polaronic states of C1–C3 and C6–C9. As for C4 and C5, only the ground state

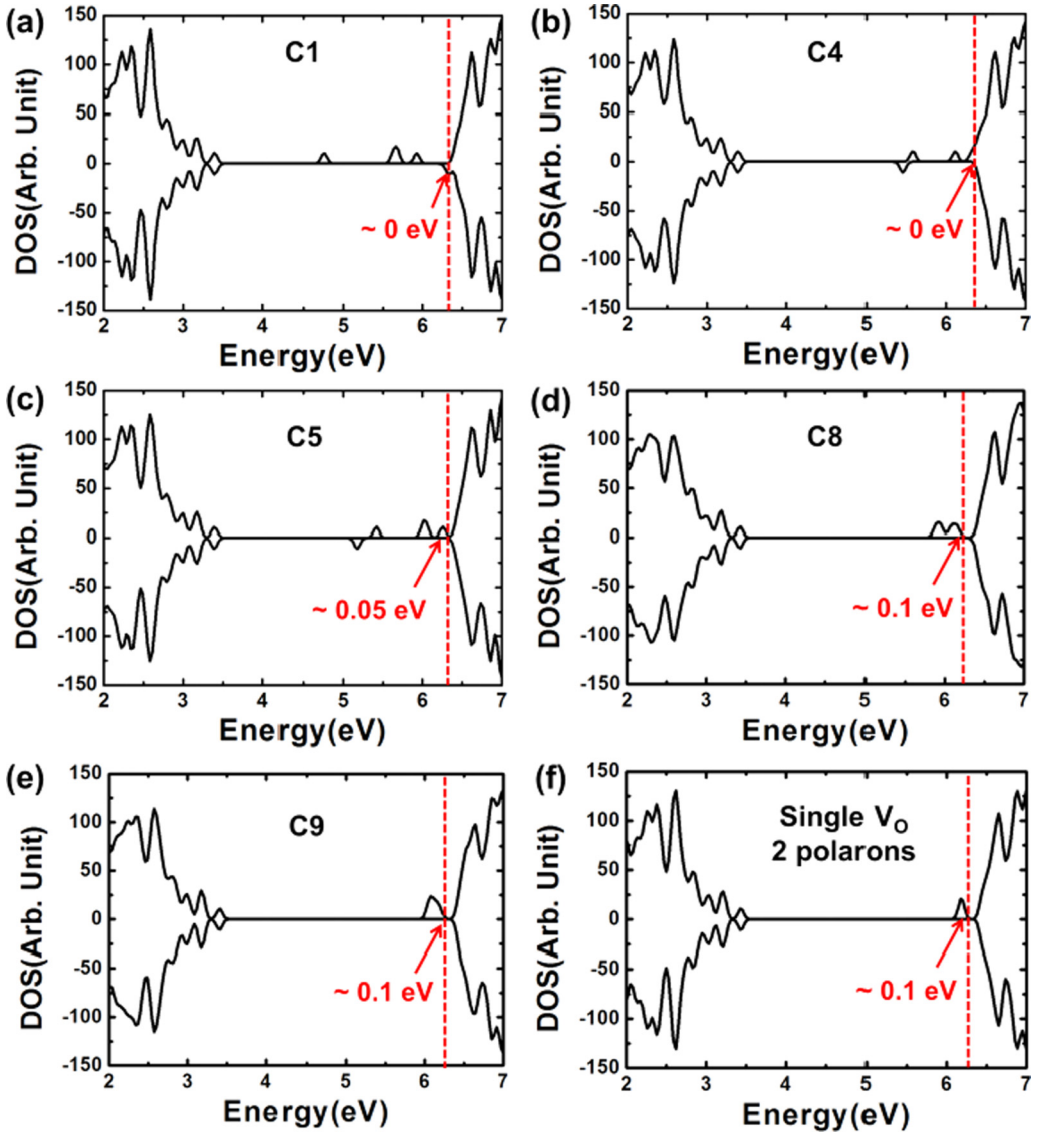

FIG. 7. Spin-dependent electron DOS of the ground state of (a) C1, (b) C4, (c) C5, (d) C8, and (e) C9. The Fermi level is represented by red dashed lines. (f) shows the DOS of the "neutral, V_O^{2+}, 2-polaron, Ti(1) and Ti(2)" state as a comparison.

is obtained from relaxations. In these cases, the ground state of each configuration always has more small polarons formed at nearby Ti atoms compared to the second-most-stable state.

At longer V_O-V_O distances (C5–C9), the ELF exhibits similar patterns as two isolated "neutral, 2-polaron" states. In these cases, the lowering of interaction energies can be attributed to the reduction of Coulomb repulsion through charge redistribution. On the other hand, at smaller V_O-V_O distances (C1–C3) the ground state no longer resembles two "neutral, V_O^{2+}, 2-polaron" states, since the two V_O share the same Ti atom as their nearest neighbor. Now the two vacancies must eject at least one electron polaron to a distant Ti atom to reach the ground state. In these cases, the lowering of interaction energies is partly due to the reduction of Coulomb repulsion and partly due to the sharing of lattice distortion between two V_O.

It is worth noting that this work is primarily focused on systems with one or two polarons. The ELF suggests that the ground state usually has the polarons localized in the close vicinity of the V_O. In previous studies, it has been shown that polarons can be rather mobile in rutile TiO_2 [56,69] and not necessarily bound to V_O. For future studies, it would be interesting to check if this is still the case for systems with a larger V_O concentration (e.g., the Magnéli phases).

Finally, we would like to discuss the effects of polaronic interactions on the conductivity of TiO_2. Figure 7 shows the spin-polarized electron DOS of configurations C1, C4, C5, C8, and C9, chosen to represent various V_O-V_O distances. The positions of defect levels are quite different in these cases: (1) C1, C4, and C5 [Figs. 7(a)–7(c)] exhibit very strong V_O-V_O interactions. Defect states are considerably split and the highest defect levels merge with the CBM. (2) C8 [Fig. 7(d)] has two oxygen vacancies that are farther apart (~ 6 Å). The splitting of defect states is still observed but to a lesser extent compared to C1, C4, and C5. The highest defect level is located at 0.1 eV below CBM, similar to the "neutral, V_O^{2+}, 2-polaron" state of a single V_O. (3) C9 [Fig. 7(e)] has two well-separated V_O (~9 Å), and its DOS looks similar to the

"neutral, V_O^{2+}, 2-polaron" state [Fig. 7(f)]. These observations suggest that stronger V_O-V_O interaction leads to shallower defect states. Since shallower defect states have lower donor activation energies, we may conclude that the clustering of oxygen vacancies will increase the conductivity of rutile TiO_2.

V. CONCLUSIONS

In this work, we report an in-depth study of the vacancy-vacancy interactions in rutile TiO_2 using density functional theory with on-site Coulomb corrections (DFT + U) and extensive search of potential polaronic states. The stability of the divacancy systems in each polaronic state is determined, and the ground state at each vacancy-vacancy distance is predicted.

Our results suggest that polaron formation plays a crucial role in the formation and interactions of oxygen vacancies in rutile TiO_2. Two isolated vacancies exhibit attractive interactions, with an equilibrium distance at about 4 Å. The attractive forces between vacancies arise from the polaronic effects, which redistribute the excess electrons to minimize their Coulomb repulsion. These discoveries provide further understanding of the vacancy clustering phenomena from a microscopic point of view.

ACKNOWLEDGMENTS

This work is supported by the Stanford nonvolatile memory research initiative (NMTRI). The DFT calculations were partly carried out at the NNIN Computing Facility of Stanford University. This work also used the Extreme Science and Engineering Discovery Environment (XSEDE) which is supported by the National Science Foundation through Grant No. ACI-1053575, and the Center for Nanoscale Materials, which is supported by the U.S. Department of Energy under Contract No. DE-AC02-06CH11357.

[1] A. L. Linsebigler, G. Lu, and J. T. Yates, Jr., Chem. Rev. **95**, 735 (1995).
[2] M. Ni, M. K. H. Leung, D. Y. C. Leung, and K. A. Sumathy, Renewable Sustainable Energy Rev. **11**, 401 (2007).
[3] R. Asahi, T. Morikawa, T. Ohwaki, K. Aoki, and Y. Taga, Science **293**, 269 (2001).
[4] S. U. M. Khan, M. Al-Shahry, Jr., and W. B. Ingler, Science **297**, 2243 (2002).
[5] S. G. Kumar and L. G. Devi, J. Phys. Chem. A **115**, 13211 (2011).
[6] G. K. Mor, K. Shankar, M. Paulose, O. K. Varghese, and C. A. Grimes, Nano Lett. **6**, 215 (2006).
[7] K. Zhu, N. R. Neale, A. Miedaner, and A. J. Frank, Nano Lett. **7**, 69 (2007).
[8] M. Kadoshima, M. Hiratani, Y. Shimamoto, K. Torii, H. Miki, S. Kimura, and T. Nabatame, Thin Solid Films **424**, 224 (2003).
[9] I. G. Baek, M. S. Lee, S. Seo, M. J. Lee, D. H. Seo, D.-S. Suh, J. C. Park, S. O. Park, H. S. Kim, I. K. Yoo, U.-I. Chung, and J. T. Moon, in *IEEE International Electron Devices Meeting*, IEDM Technical Digest (IEEE, 2004), p. 587.
[10] D. B. Strukov, G. S. Snider, D. R. Stewart, and R. Stanley Williams, Nature (London) **453**, 80 (2008).
[11] D.-H. Kwon, K. M. Kim, J. H. Jang, J. M. Jeon, M. H. Lee, G. H. Kim, X.-S. Li, G.-S. Park, B. Lee, S. Han, M. Kim, and C. S. Hwang, Nat. Nanotechnol. **5**, 148 (2010).
[12] H.-S. P. Wong, H.-Y. Lee, S. Yu, Y.-S. Chen, Y. Wu, P.-S. Chen, B. Lee, F. T. Chen, and M.-J. Tsai, Proc. IEEE **100**, 1951 (2012).
[13] E. Yagi, R. R. Haiguti, and M. Aono, Phys. Rev. B **54**, 7945 (1996).
[14] L. Forro, O. Chauvet, D. Emin, L. Zuppiroli, H. Berger, and F. Levy, J. Appl. Phys. **75**, 633 (1994).
[15] M. K. Nowotny, T. Bak, and J. Nowotny, J. Phys. Chem. B **110**, 16270 (2006).
[16] N. A. Deskins, R. Rousseau, and M. Dupuis, J. Phys. Chem. C **114**, 5891 (2010).
[17] A. Janotti, C. Franchini, J. B. Varley, G. Kresse, and C. G. Van de Walle, Phys. Status Solidi RRL **7**, 199 (2013).
[18] I. G. Austin and N. F. Mott, Adv. Phys. **18**, 41 (1969).
[19] S. Yang, A. T. Brant, N. C. Giles, and L. E. Halliburton, Phys. Rev. B **87**, 125201 (2013).
[20] S. Andersson, B. Collen, U. Kuylenstierna, and A. Magnéli, Acta Chem. Scand. **11**, 1641 (1957).
[21] J. Y. Shin, J. H. Joo, D. Samuelis, and J. Maier, Chem. Mater. **24**, 543 (2012).
[22] W.-Q. Han and Y. Zhang, Appl. Phys. Lett. **92**, 203117 (2008).
[23] X. Tao, J. Wang, Z. Ying, Q. Cai, G. Zheng, Y. Gan, and Y. Cui, Nano Lett. **14**, 5288 (2014).
[24] J. R. Smith, F. C. Walsh, and R. L. Clarke, J. Appl. Electrochem. **28**, 1021 (1998).
[25] T. Ioroi, Z. Siroma, N. Fujiwara, S. I. Yamazaki, and K. Yasuda, Electrochem. Commun. **7**, 183 (2005).
[26] R. F. Bartholomew and D. R. Frankl, Phys. Rev. **187**, 828 (1969).
[27] I. Leonov, A. N. Yaresko, V. N. Antonov, U. Schwingenschlögl, V. Eyert, and V. I. Anisimov, J. Phys.: Condens. Matter **18**, 10955 (2006).
[28] L. Liborio and N. Harrison, Phys. Rev. B **77**, 104104 (2008).
[29] L. Liborio, G. Mallia, and N. Harrison, Phys. Rev. B **79**, 245133 (2009).
[30] M. Weissmann and R. Weht, Phys. Rev. B **84**, 144419 (2011).
[31] S. G. Park, B. Magyari-Köpe, and Y. Nishi, Phys. Rev. B **82**, 115109 (2010).
[32] L. Zhao, S. G. Park, B. Magyari-Köpe, and Y. Nishi, Math. Comput. Model. **58**, 275 (2013).
[33] S. Lany and A. Zunger, Phys. Rev. B **80**, 085202 (2009).
[34] S. Lany, Phys. Status Solidi B **248**, 1052 (2011).
[35] P. Deak, B. Aradi, and T. Frauenheim, Phys. Rev. B **83**, 155207 (2011).
[36] P. Deak, B. Aradi, and T. Frauenheim, Phys. Rev. B **86**, 195206 (2012).
[37] A. Janotti, J. B. Varley, P. Rinke, N. Umezawa, G. Kresse, and C. G. Van de Walle, Phys. Rev. B **81**, 085212 (2010).
[38] H.-Y. Lee, S. J. Clark, and J. Robertson, Phys. Rev. B **86**, 075209 (2012).
[39] J. Robertson and R. Gillen, Microelectron. Eng. **109**, 208 (2013).
[40] E. Finazzi, C. Di Valentin, G. Pacchioni, and A. Selloni, J. Chem. Phys. **129**, 154113 (2008).

[41] B. J. Morgan and G. W. Watson, Phys. Rev. B **80**, 233102 (2009).
[42] H. Kamisaka, T. Suenaga, H. Nakamura, and K. Yamashita, J. Phys. Chem. C **114**, 12777 (2010).
[43] N. Umezawa and J. Ye, Phys. Chem. Chem. Phys. **14**, 5924 (2012).
[44] T. S. Bjørheim, A. Kuwabara, and T. Norby, J. Phys. Chem. C **117**, 5919 (2013).
[45] A. M. Czoska, S. Livraghi, M. Chiesa, E. Giamello, S. Agnoli, G. Granozzi, E. Finazzi, C. Di Valentin, and G. Pacchioni, J. Phys. Chem. C **112**, 8951 (2008).
[46] A. T. Brant, E. M. Golden, N. C. Giles, S. Yang, M. A. R. Sarker, S. Watauchi, M. Nagao, I. Tanaka, D. A. Tryk, A. Manivannan, and L. E. Halliburton, Phys. Rev. B **89**, 115206 (2014).
[47] S. Yang, L. E. Halliburton, A. Manivannan, P. H. Bunton, D. B. Baker, M. Klemm, S. Horn, and A. Fujishima, Appl. Phys. Lett. **94**, 162114 (2009).
[48] F. D. Brandao, M. V. B. Pinheiro, G. M. Ribeiro, G. Medeiros-Ribeiro, and K. Krambrock, Phys. Rev. B **80**, 235204 (2009).
[49] A. T. Brant, N. C. Giles, S. Yang, M. A. R. Sarker, S. Watauchi, M. Nagao, I. Tanaka, D. A. Tryk, A. Manivannan, and L. E. Halliburton, J. Appl. Phys. **114**, 113702 (2013).
[50] E. Kioupakis, P. Rinke, A. Janotti, Q. Yan, and C. G. Van de Walle, in *Computational Approaches to Energy Materials* (John Wiley & Sons Ltd., Oxford, UK, 2013), Chap. 8.
[51] G. Kresse and J. Hafner, Phys. Rev. B **47**, 558 (1993); **49**, 14251 (1994).
[52] P. E. Blochl, Phys. Rev. B **50**, 17953 (1994).
[53] V. I. Anisimov and O. Gunnarsson, Phys. Rev. B **43**, 7570 (1991).
[54] I. A. Nekrasov, M. A. Korotin, and V. I. Anisimov, arXiv:cond-mat/0009107.
[55] L. Zhao, S. G. Park, B. Magyari-Köpe, and Y. Nishi, Appl. Phys. Lett. **102**, 083506 (2013).
[56] M. Setvin, C. Franchini, X. Hao, M. Schmid, A. Janotti, M. Kaltak, C. G. Van de Walle, G. Kresse, and U. Diebold, Phys. Rev. Lett. **113**, 086402 (2014).
[57] M. Cococcioni and S. de Gironcoli, Phys. Rev. B **71**, 035105 (2005).
[58] A. D. Becke, J. Chem. Phys. **92**, 5397 (1990).
[59] N. A. Deskins and M. Dupuis, Phys. Rev. B **75**, 195212 (2007).
[60] S. P. Ong, V. L. Chevrier, and G. Ceder, Phys. Rev. B **83**, 075112 (2011).
[61] H. Ding, H. Lin, B. Sadigh, F. Zhou, V. Ozoliņš, and M. Asta, J. Phys. Chem. C **118**, 15565 (2014).
[62] G. Wang, H. Wang, Y. Ling, Y. Tang, X. Yang, R. C. Fitzmorris, C. Wang, J. Z. Zhang, and Y. Li, Nano Lett. **11**, 3026 (2011).
[63] F. Zuo, L. Wang, T. Wu, Z. Zhang, D. Borchardt, and P. Feng, J. Am. Chem. Soc. **132**, 11856 (2010).
[64] T. Shibuya, K. Yasuoka, S. Mirbt, and B. Sanyal, J. Phys.: Condens. Matter **24**, 435504 (2012).
[65] T. Shibuya, K. Yasuoka, S. Mirbt, and B. Sanyal, J. Phys. Chem. C **118**, 9429 (2014).
[66] N. A. Deskins, R. Rousseau, and M. Dupuis, J. Phys. Chem. C **115**, 7562 (2011).
[67] X. Hao, Z. Wang, M. Schmid, U. Diebold, and C. Franchini, Phys. Rev. B **91**, 085204 (2015).
[68] P. W. Atkins and J. De Paula, *Physical Chemistry: Thermodynamics, Structure, and Change*, 10th ed. (W. H. Freeman and Company, New York, 2014).
[69] P. M. Kowalski, M. F. Camellone, N. N. Nair, B. Meyer, and D. Marx, Phys. Rev. Lett. **105**, 146405 (2010).